Biointerface Research in Applied Chemistry
Open-Access Journal (ISSN: 2069-5837)

Article
Volume 13, Issue 1, 2023, 86
https://doi.org/10.33263/BRIAC131.086

Improving UV Light Photocatalytic Activity of WO_3 by Doping with Boron and Compounding with Polypyrrole

Hafize Nagehan Koysuren [1], Ozcan Koysuren [2,*]

[1] Department of Environmental Engineering, Kirsehir Ahi Evran University, Kirsehir, 40100, Turkey; hnkoysuren@gmail.com (H.N.K.);
[2] Department of Energy Engineering, Ankara University, Ankara, 06830, Turkey; koysuren@ankara.edu.tr (O.K.);
* Correspondence: koysuren@ankara.edu.tr (O.K.);

Scopus Author ID 12781818300
Received: 6.12.2021; Accepted: 3.01.2022; Published: 12.06.2022

Abstract: Tungsten oxide (WO_3) and boron-doped WO_3 (WO_3-B) nanoparticles were synthesized using the co-precipitation technique. In addition, as-prepared photocatalysts were compounded with a conducting polymer, polypyrrole (PPy), to prepare PPy/WO_3 and PPy/WO_3-B composites. The photocatalytic activity of pure WO_3, WO_3-B, and the PPy composites for decomposing an organic dye, methylene blue, was compared. Doping with boron atoms and/or compounding with polypyrrole improved the photocatalytic performance of WO_3, which was probed by performing UV-Vis absorption spectroscopy. The boron doping improved the photocatalytic performance of the WO_3 nanoparticles, which was ascribed to reducing the recombination rate of the photoinduced charge carriers and the increase in the number of photogenerated holes on WO_3 upon UV light irradiation. Compounding WO_3 with polypyrrole enhanced the photocatalytic activity, which was also assigned to the decrease in the recombination rate of the photoexcited charge carriers.

Keywords: WO_3; boron doping; polypyrrole; photocatalytic activity; polymer composite.

1. Introduction

Different industries, especially the fabric and leather industries, continue to increase their production, increasing the discharge rate of the wastewater with pollutants. Industries utilize various types of organic dyes that are highly toxic and can cause serious effects on humans and other living organisms. To diminish the negative effects of the organic pollutants on the human being and the environment, industrial wastewater must be properly treated before being released into the environment [1]. Many studies have been carried out to develop efficient technologies to reduce the amount of wastewater released and enhance the quality of the wastewater by reducing the number of pollutants within it. Numerous efforts have been attempted to develop efficient technologies to decrease the amount of wastewater produced and increase the quality of the treated water [2]. Photocatalytic decomposition of organic molecules under UV light or visible light in the presence of a semiconductor photocatalyst has been known as a considerable technique for removing organic pollutants from wastewater. In the last years, significant attempts have been performed to synthesize high-efficient photocatalysts to remove the organic pollutants from the wastewater through photocatalytic decomposition [3].

Among the photocatalysts researched, TiO_2 [4] and ZnO [5] have been the most preferred ones used to decompose the organic pollutants within the wastewater. The main drawback of the specified photocatalysts is that they can absorb a narrow wavelength region of the natural sunlight owing to their wider optical band gaps and utilized in photocatalytic degradation reactions. To utilize the sunlight more effectively and enhance the photocatalytic activity, it is required to extend the absorption capability of the photocatalyst to the long-wavelength region greater than 387 nm. Tungsten oxide (WO_3) with an optical band gap of 2.4-2.8 eV can benefit much more from the sunlight [1]. Owing to its favorable hole diffusion lengths, WO_3 can benefit almost 12% of the sunlight [6]. Possessing unique optoelectronic properties, WO_3 has been utilized in various fields such as dye-sensitized solar cells, gas sensors, and lithium-ion batteries [1,6]. WO_3 can also be utilized as a catalyst for hydrogen energy production [7].

The fast recombination of photoexcited charge carriers on the semiconductor photocatalysts suppresses the photocatalytic activity and limits their application potential in removing the organic pollutants from the wastewater [3]. WO_3 exhibits poor photocatalytic performance in the degradation of organic pollutants due to its sluggish kinetics, resulting in slow charge transfer at the photocatalyst-wastewater interface [6]. To enhance the photocatalytic performance of WO_3, different strategies have been followed by the scientists who studied this topic [3]. Combining WO_3 with a conducting polymer, such as polypyrrole [8], polyaniline [9], and polythiophene [10] are among the strategies applied. The composite application can enhance the photocatalytic performance of WO_3 by promoting interfacial electron transfer and harvesting more sunlight. Any effect that provides electron transfer from the conduction band or valence band of WO_3 also reduces the recombination rate of the photoinduced charge carriers [7]. Polypyrrole has attracted more attention among the conducting polymers due to its unique properties such as chemical stability, relatively high electrical conductivity, redox property, and simplicity of its synthesis [8,11]. In the literature, TiO_2 [12], Ag [8], ZnO [5], Fe_3O_4 [5], g-C_3N_4 [13], Bi_2O_4 [14], graphene oxide [15], CuO [16], Fe_2O_3 [17], Ag_3PO_4 [18], Bi_2MoO_6 [19], ZnTi [20], SnO_2 [21] and $BiVO_4$ [22] have been studied to prepare their composites with the conducting polymer, polypyrrole. With its highly conductive structure, polypyrrole allows interfacial electron transfer depending on its band energy levels, reducing the photoexcited charge carriers on WO_3.

Alternatively, the photocatalytic performance of WO_3 can be improved by increasing the lifetime of the photoexcited charge carriers and suppressing the recombination rate, which can be achieved by metal or nonmetal doping. WO_3 can absorb the solar spectrum's UV light, blue light, and green light regions (up to 516 nm). To enhance the visible light sensitivity and photocatalytic performance, the optical band gap of WO_3 can be narrowed. The optical band gap of WO_3 can be effectively narrowed by metal or nonmetal doping. In literature, the metal or nonmetal doping with sulfur atoms [3], Mg atoms [23], Au atoms [24], Ag atoms [25], Zn atoms, and Cu atoms [26] has been employed to tailor the optical band gap and to enhance the separation of the photoexcited charge carriers. Among different metal or nonmetal atoms used as a dopant, several attempts have been performed to obtain boron-doped TiO_2 [27], ZnO [28], BiOBr [29], and Bi_2WO_6 [30]. Boron atoms can disturb the crystal growth and introduce energy levels into the bandgap of the semiconductor photocatalyst, which gives rise to the reduction in the optical band gap energy and enhancement in the photocatalytic activity.

Within the scope of this study, boron doping was applied to the WO_3 nanoparticles. In addition, pure and boron-doped WO_3 nanoparticles were compounded with polypyrrole

separately. The photocatalytic activity of the doped WO_3 and polypyrrole composites were analyzed and compared with pure WO_3 by monitoring the degradation of the model dye, methylene blue, in an aqueous solution under UV light irradiation. Doping WO_3 with boron atoms and/or compounding WO_3 with polypyrrole seemed to be efficient techniques to enhance the photocatalytic activity of WO_3. To the best of our knowledge, the study on the effect of boron doping on the photocatalytic activity of WO_3 and the PPy/WO_3 composite has not been reported so far.

2. Materials and Methods

WO_3 nanoparticles were synthesized following the co-precipitation technique. Chemicals used to synthesize WO_3 nanoparticles were purchased from Sigma-Aldrich. In detail, sodium tungstate dihydrate ($Na_2WO_4 \cdot 2H_2O$) (3 g) was dissolved in distilled water (20 ml) and kept under stirring at room temperature using a magnetic stirrer. Meanwhile, 8 M HCl solution (20 ml) was prepared and poured into the sodium tungstate dihydrate solution. The as-prepared solution was stirred for 2 hours at 80 °C and then left to cool. Hence, a slurry, including amorphous WO_3 structures, was obtained. The as-prepared slurry was separated from the solution and cleaned thoroughly, washing with distilled water. Afterward, the slurry was dried at 80°C for 12 hours and then calcined at 600°C for 1 hour to convert the amorphous WO_3 phase into the crystalline phase. Following the calcination process, WO_3 crystallites were grounded. Finally, WO_3 nanoparticles were obtained [31]. Boron doped WO_3 (WO_3-B) was also synthesized using the co-precipitation technique in the presence of a boron atom source, boric acid. In detail, a certain amount of boric acid was added to the sodium tungstate dehydrate solution and stirred for 30 minutes. Then, 8 M HCl solution was poured into the as-prepared solution, including boric acid. The solution was stirred for 2 h at 80°C. Then the solution was left to cool. Thus, a slurry phase was obtained. The resulting slurry was separated from the acid solution and rinsed with distilled water. Afterward, the slurry was dried at 80°C for 12 hours and then calcined at 600°C for 1 hour. Following the specified technique, WO_3-B nanoparticles, including 1 wt.% of a boron atom, were obtained [27,31].

PPy/WO_3 and PPy/WO_3-B composites, including 50 wt.% of WO_3 and WO_3-B, respectively, were prepared using the in-situ polymerization technique. The conducting polymer, polypyrrole, was synthesized in the presence of WO_3 (or WO_3-B) nanoparticles through the oxidation of the monomer (pyrrole) with an oxidant (iron(III) oxide hexahydrate). All chemicals used to synthesize the PPy composites were purchased from Sigma-Aldrich. For this purpose, 0.7 ml (10 mmol) of pyrrole was dispersed in 100 ml of distilled water. A certain amount of WO_3 (or WO3-B) nanoparticles were added to the pyrrole solution and stirred for 30 minutes. In accordance with the stoichiometric ratio ([$FeCl_3$]/[pyrrole] = 2.5), 6.76 g (25 mmol) of iron(III) oxide hexahydrate was added into the pyrrole solution. The solution was stirred at room temperature for 24 hours. Following 24 hours of stirring, a solid composite phase was obtained. The resulting composite phase was separated from the solution through filtration. Afterward, the composite particles were rinsed with 0.1 M hydrochloric acid and acetone. The PPy/WO_3 and PPy/WO_3-B composites were obtained after drying at room temperature [32].

The optical properties of all samples were investigated using UV-Vis absorption spectroscopy (Genesys 10S, Thermo Scientific). Photocatalytic activity of all samples was evaluated by monitoring the decomposition of the model dye, methylene blue, in an aqueous solution under UV light irradiation. 0.5 g of the photocatalyst sample was dispersed in 100 ml

of the dye solution (10 mg/l). The dye solution, including the photocatalyst, was stirred in the dark for half an hour using a magnetic stirrer. Then, the dye solution was irradiated using a UVA lamp (12 W) under stirring. Samples (3 ml) were collected every 20 min. and centrifuged to separate the solution from the photocatalyst particles. The clarified solution was analyzed using the UV–Vis spectrophotometer (Genesys 10S, Thermo Scientific). The absorbance of methylene blue, measured at 664 nm, was used to calculate the degradation efficiency using the following equation [12]:

$$\text{Degradation efficiency (\%)} = (A_0\text{-}A)/A_0 \quad (1)$$

Where A_0 is the initial absorbance of methylene blue, and A is the absorbance of methylene blue after irradiation. In addition, to reveal the degradation mechanism of the photocatalyst samples, ammonium oxalate (1 mM) as a hole scavenger (h^+) and potassium persulfate (1 mM) as an electron scavenger were added into the dye solution of WO_3-B and PPy/WO_3-B.

3. Results and Discussion

3.1. UV-Vis spectroscopy.

The UV–Vis absorption spectra of WO_3-B, PPy/WO_3, and PPy/WO_3-B were compared with pure WO_3 in Figure 1. It was observed that the photo-response of WO_3 nanoparticles doped with boron atoms shifted slightly into the visible spectrum. The reason for the red-shift might be the formation of energy levels in the bandgap of WO_3 due to the diffusion of boron atoms through the interstitial of the crystal lattice [33].

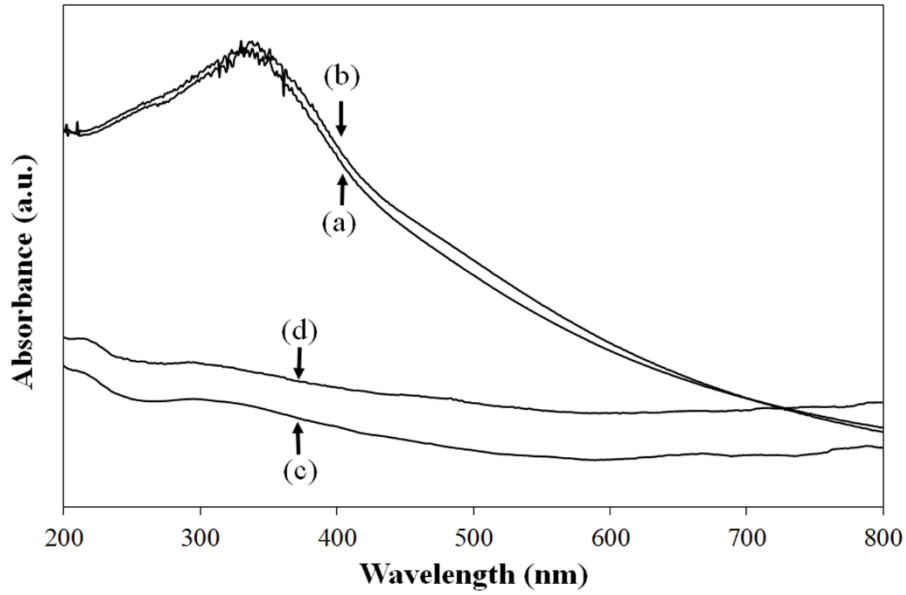

Figure 1. UV-Vis absorbance spectra of (a) WO_3, (b) WO_3-B, (c) PPy/WO_3, and (d) PPy/WO_3-B.

PPy composites exhibited wide absorption starting from the UV spectrum to the visible spectrum up to 600 nm. The absorption spectrum of PPy/WO_3-B was also broad and slightly red-shifted compared with PPy/WO_3. The optical band gap energies (E_g) of WO_3, WO_3-B, PPy–WO_3 and PPy/WO_3-B were estimated by extrapolating the linear part of the curve to the x-axis on the plot of hυ vs. $(\alpha h\nu)^2$ using the Tauc's equation (Figure 2) [33]:

$$\alpha h\upsilon = A(h\upsilon - E_g)^{1/2} \quad (2)$$

where α, hυ, A and E_g are the absorption coefficient, the photon energy, a constant, and the optical band gap energy, respectively [33]. The estimated bandgap energy for WO_3, WO_3-B,

PPy/WO_3, and PPy/WO_3-B was 2.75 eV, 2.70 eV, 2.60 eV, and 2.45 eV, respectively. According to these results, the bandgap energies of the PPy composites are lower than that of WO_3 nanoparticles. Upon the boron doping of WO_3, further reduction in the bandgap energy for WO_3 and PPy/WO_3 was observed, indicating that the boron atoms were integrated into the interstitial sites WO_3 crystal lattice successfully.

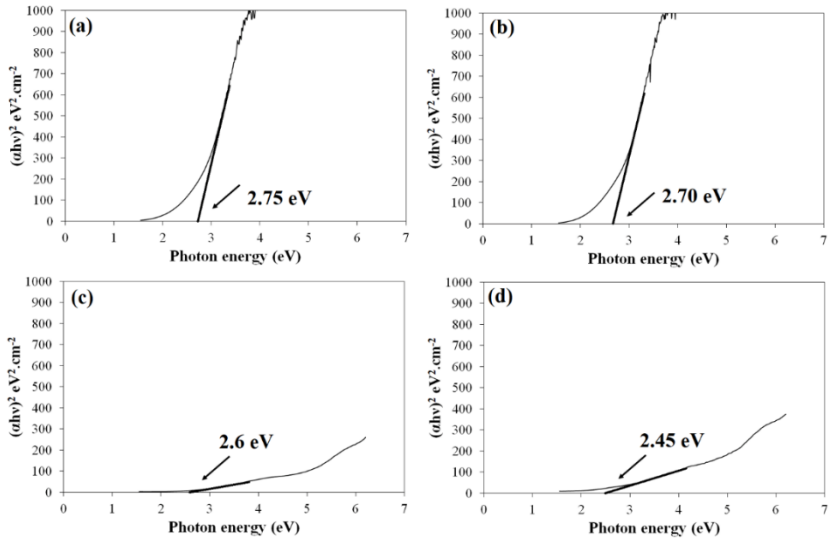

Figure 2. Tauc's plot for (a) WO_3, (b) WO_3-B, (c) PPy/WO_3, and (d) PPy/WO_3-B.

3.2. Photocatalytic activity.

The photocatalytic degradation reactions start with the formation of electrons and holes on the conduction band and the valence band, respectively, when the photocatalyst is irradiated with UV or visible light. Afterward, the electrons and holes can react with surface adsorbed O_2 and H_2O molecules to form superoxide anion radicals ($\bullet O_2^-$) and hydroxyl radicals (•OH) radicals, respectively. These strong radicals can decompose the organic dye molecules into small molecules such as H_2O and CO_2 [8]. The photocatalytic activity of as-prepared samples was evaluated through the degradation of methylene blue in an aqueous solution. Figure 3 illustrates the decline in the absorption of the model dye under UV light irradiation. Methylene blue was degraded 10.9% by boron-doped WO_3 within 80 minutes. With the boron doping, approximately 3% more methylene blue decomposition was obtained at the end of the UV light irradiation (80 min.) (Figure 4). Boron atoms might diffuse through the interstitial sites of the WO_3 crystal lattice. The diffusion of boron atoms through the interstitial sites of the WO_3 lattice could reduce the optical band gap energy by forming energy levels between the conduction band and the valence band of WO_3 [34]. The boron doping might result in the formation of electron-empty acceptor levels located above the valence band of WO_3, known as hole traps. These hole traps accept electrons; if the energy difference between the valence band edge and the hole traps is smaller than the thermal energy of the electrons, the electrons in the valence band can be thermally excited to these hole traps, resulting in the formation of additional holes to participate in the oxidation reactions [35]. On the other hand, these hole traps can accept photoexcited electrons from the conduction band. Eventually, the electrons trapped by these energy states above the valence band recombine with the holes. The excitation of valence band electrons to the conduction band and simultaneous formation of holes in the valence band occurs in femtoseconds. On the other hand, the trapping of the photoexcited electrons can happen on a time scale of seconds to minutes, reducing the recombination rate of the

photoinduced charge carriers [35]. Hence, the improvement in the photocatalytic activity might be attributed to the electron traps formed with the boron doping. Boron doping was thought to improve photocatalytic performance by increasing the number of holes in the valence band of WO_3 and reducing the recombination rate of the photogenerated electron-hole pairs formed on WO_3.

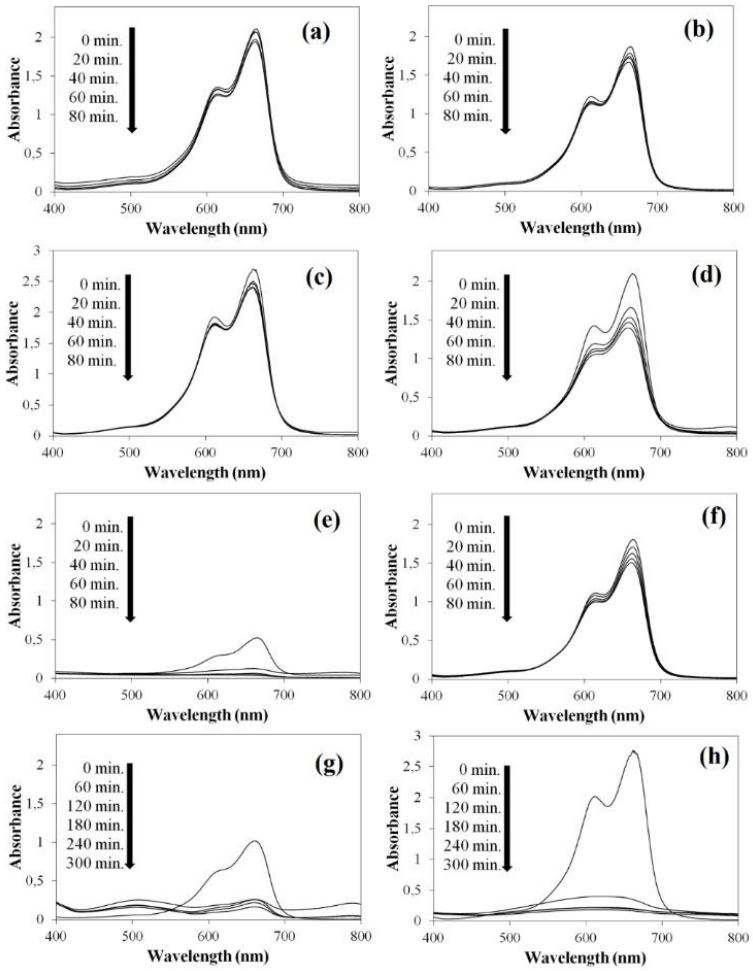

Figure 3. The variation in the UV–visible spectrum of the dye solution including (a) WO_3, (b) WO_3-B, (c) PPy/WO_3, (d) PPy/WO_3-B, (e) WO_3-B with e^- scavenger, (f) WO_3-B with h^+ scavenger, (g) PPy/WO_3-B with e^- scavenger and (h) PPy/WO_3-B with h^+ scavenger.

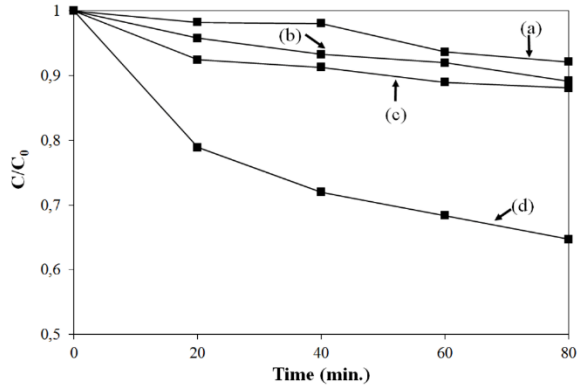

Figure 4. Degradation efficiency of methylene blue (a) WO_3, (b) WO_3-B, (c) PPy/WO_3, and (d) PPy/WO_3-B under UVA light irradiation.

To understand the photocatalytic mechanism of the boron doped WO_3 nanoparticles, the effect of electron and hole scavengers on the decomposition of methylene blue molecules

was studied. The addition of the electron and hole scavengers significantly affected the decomposition of the model dye. Methylene blue was degraded 93.4% and 17.1% within 80 minutes by the WO_3-B nanoparticles in the presence of e^- and h^+ scavengers, respectively (Figure 5). The enhancement in the photocatalytic activity indicated that the photoinduced electrons and holes were effective in the photocatalytic decomposition of organic dye molecules. It was expected that the scavengers might hold the photoexcited electrons or holes, leading to a decrease in the recombination rate and an increase in the number of charge carriers. This effect of the scavengers might increase the number of active radicals, decompose the organic dye molecules, and enhance photocatalytic activity. When both scavengers were compared, the electron scavenger seemed to be more effective, which was attributed to the fact that the photoexcited holes were more effective in degrading the organic pollutant. The low reduction potential of the photoinduced electrons of WO_3 might reduce the formation rate of superoxide anion radicals and the following decomposition reactions on the conduction band [36]. On the other hand, boron doping might increase the number of holes by introducing energy levels above the valence band of WO_3. This fact also revealed that the photoinduced holes were taken a more active role in the degradation reactions. The low photocatalytic performance of pure WO_3 nanoparticles might be attributed to the low reduction potential of electrons on the conduction band and the high recombination rate of the photoexcited electron-hole pairs.

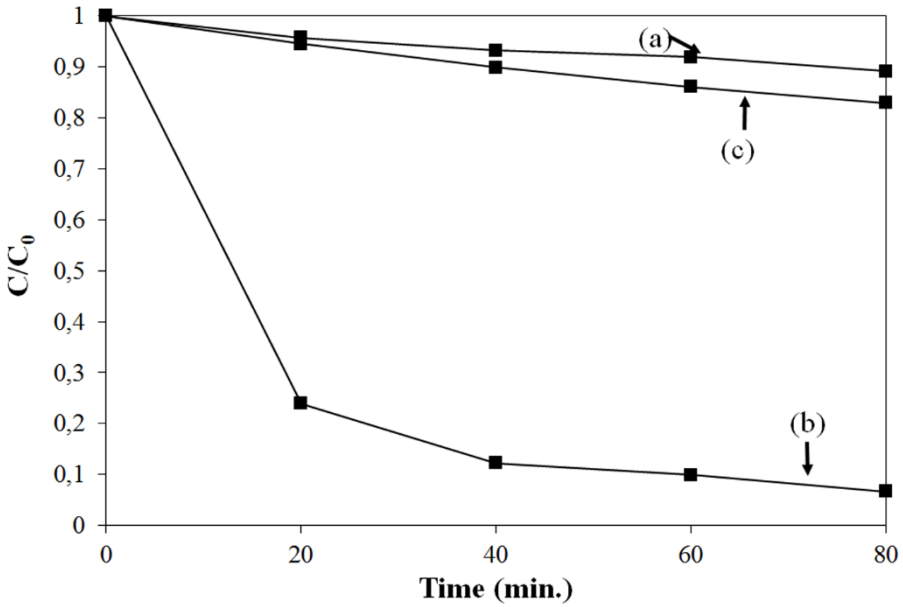

Figure 5. The degradation efficiency of methylene blue over (a) WO_3-B without scavenger, (b) WO_3-B with e^- scavenger, and (c) WO_3-B with h^+ scavenger under UVA light irradiation.

The photocatalytic degradation of methylene blue in the presence of PPy/WO_3 composites was enhanced compared to pure WO_3. Methylene blue was degraded 12.0% with PPy/WO_3 composite. The highest degradation rate was obtained with PPy/WO_3-B composite. 35.4% of methylene blue in the aqueous solution was decomposed on the composite surface after 80 minutes of UV light irradiation (Figure 4). This improvement was assigned to reducing the recombination rate of the photoinduced charge carriers of WO_3. According to the literature, the valence band edge of PPy is more negative than the valence band edge of WO_3. So, the photoinduced holes of WO_3 can transfer to the valence band of PPy, which can suppress the recombination of the photoexcited electron-hole pairs of WO_3. Also, the conduction band edge

of PPy is more negative compared to the conduction band edge of WO_3, which gives rise to the transfer of the photoexcited electrons from the conduction band of PPy to the conduction band of WO_3, which increases the number of electrons of WO_3 to reduce the surface adsorbed O_2 molecules [12]. Thus, combining WO_3 with PPy might lead to suppression in the recombination of the photoinduced charge carriers of WO_3 owing to the differences in the band energy levels of the composite constituents.

When the presence of scavengers on the photocatalytic activity of the PPy/WO3-B composite was examined, it was observed that the addition of the electron (e-) and hole (h+) was added scavengers enhanced the photocatalytic decomposition of the dye molecules. 84.0% and 94.1% of the organic dye were decomposed within 80 min. with e^- and h^+ scavengers, respectively (Figure 6). The enhancement in the photocatalytic decomposition revealed that both charge carriers were quite effective in the decomposition reactions. Under UV light irradiation, the photoinduced electrons of WO_3 and the electrons migrating from the conduction band of PPy might reduce the surface adsorbed O_2 to the superoxide anion radicals ($\bullet O_2^-$). On the other hand, the photoinduced holes, boron sourced and not migrated into the valence band of PPy, might oxidize the surface adsorbed H_2O to the hydroxyl radicals (•OH) [33].

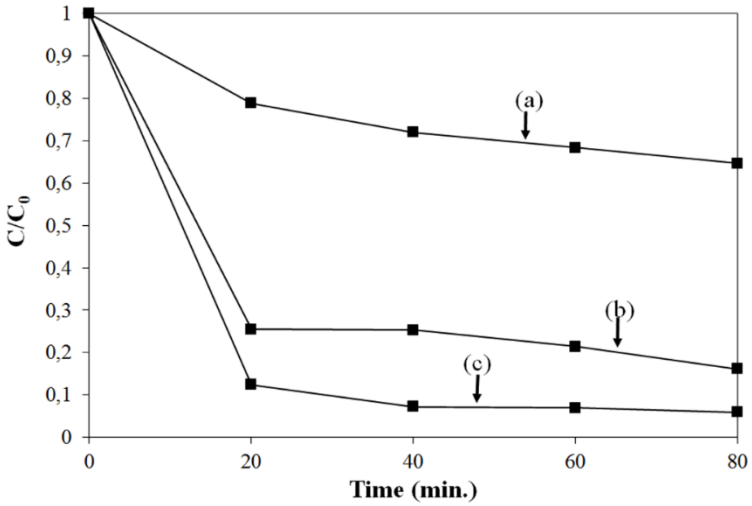

Figure 6. The degradation efficiency of methylene blue over (a) PPy/WO_3-B without scavenger, (b) PPy/WO_3-B with e^- scavenger, and (c) (PPy/WO_3-B with h^+ scavenger under UVA light irradiation.

To study the photocatalytic degradation kinetics of the organic dye in the presence of the photocatalysts, the pseudo-first-order kinetic model was used [37]:

$$\ln(C_0/C_t) = kt \quad (3)$$

Where C_0 is the concentration of the model dye before irradiation, C_t is the concentration of the model dye after irradiation, t is the time duration, and k is the rate constant, which can be obtained from the slope of the plot t vs. $\ln(C_0/C_t)$ (Figure 7). It was observed that the rate constant of WO_3-B is higher than that of pure WO_3 (Table 1). Similarly, the rate constant of PPy/WO_3-B is higher than that of the composite, including undoped WO_3 (Table 1). Compared with pure WO_3, the degradation reaction rate obtained with the PPy/WO_3-B composite increased about 6 times. High R^2 values indicated that the pseudo-first-order kinetic model could be applied to the photocatalytic decomposition reactions.

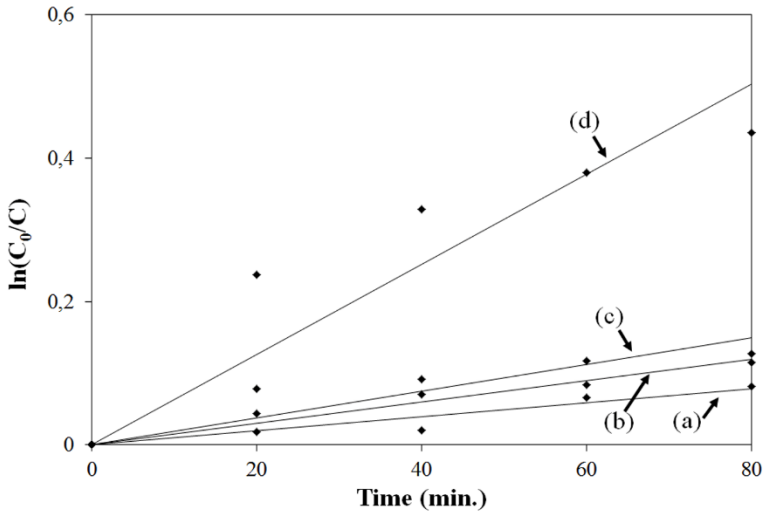

Figure 7. Photocatalytic degradation kinetics of methylene blue onto (a) WO_3, (b) WO_3-B, (c) PPy/WO_3, and (d) PPy/WO_3-B under UVA light irradiation.

Table 1. The discoloration rate of methylene blue for WO_3, WO_3-B, PPy/WO_3, and PPy/WO_3-B.

Sample	k (min^{-1})	R^2
WO_3	0.001	0.9090
WO_3-B	0.0015	0.9557
PPy/WO_3	0.0019	0.7527
PPy/WO_3-B	0.0063	0.8338

4. Conclusions

WO_3 nanoparticles were prepared using the co-precipitation method. In addition, to improve the photocatalytic performance, WO_3 was doped with boron atoms during its synthesis and then combined with polypyrrole. The photocatalytic activity of the as-prepared samples for the degradation of the model organic dye, methylene blue, under UV light irradiation was evaluated. PPy/WO3-B composite exhibited the highest photodegradation efficiency among all the samples. The degradation percentage of the model dye by the specified composite reached 35.4% after 80 min. of UV light irradiation. This improvement was ascribed to the formation of interfacial sites between the composite constituents, suppressing the recombination of the photoexcited charge carriers on WO_3. In addition, doping WO_3 with boron atoms improved the photocatalytic activity by increasing the number of holes in the valence band of WO_3 and reducing the recombination rate of the photogenerated electron-hole pairs formed on WO_3.

Funding

This research received no external funding.

Acknowledgments

This research has no acknowledgment.

Conflicts of Interest

The authors declare no conflict of interest.

References

1. Palanisamy, G.; Bhuvaneswari, K.; Pazhanivel, T.; Bharathi, G. Enriched photocatalytic activity of Rhodamine B dye from aqueous solution using hollow sphere tungsten trioxide nanoparticles. *Optik* **2020**, *204*, https://doi.org/10.1016/j.ijleo.2020.164171.
2. Palanisamy, G.; Bhuvaneswari, K.; Bharathi, G.; Nataraj, D.; Pazhanivel, T. Enhanced Photocatalytic Properties of ZnS-WO3 Nanosheet Hybrid under Visible Light Irradiation. *Chemistryselect* **2018**, *3*, 9422-9430, https://doi.org/10.1002/slct.201801688.
3. Chen, G.D.; Wang, Q.; Zhao, Z.L.; Gao, L.; Li, X.C. Synthesis and photocatalytic activity study of S-doped WO3 under visible light irradiation. *Environ. Sci. Pollut. Res.* **2020**, *27*, 15103-15112, https://doi.org/10.1007/s11356-020-07827-z.
4. Yuan, X.J.; Kobylanski, M.P.; Cui, Z.P.; Li, J.; Beaunier, P.; Dragoe, D.; Colbeau-Justin, C.; Zaleska-Medynska, A.; Remita, H. Highly active composite TiO2-polypyrrole nanostructures for water and air depollution under visible light irradiation. *J. Environ. Chem. Eng.* **2020**, *8*, https://doi.org/10.1016/j.jece.2020.104178.
5. Nayebi, P.; Babamoradi, M. Synthesis of ZnO nanorods/Fe3O4/polypyrrole nanocomposites for photocatalytic activity under the visible light irradiation. *Optik* **2021**, *244*, https://doi.org/10.1016/j.ijleo.2021.167497.
6. Lei, R.; Zhang, H.; Ni, H.W.; Chen, R.S.; Gu, H.Z.; Zhang, B.W. Novel ZnO nanoparticles modified WO3 nanosheet arrays for enhanced photocatalytic properties under solar light illumination. *Applied Surface Science* **2019**, *463*, 363-373, https://doi.org/10.1016/j.apsusc.2018.08.218.
7. Tahir, M.B.; Sagir, M.; Abas, N. Enhanced photocatalytic performance of CdO-WO3 composite for hydrogen production". *Int. J. Hydrog. Energy* **2019**, *44*, 24690-24697, https://doi.org/10.1016/j.ijhydene.2019.07.220.
8. Punnakkal, V.S.; Jos, B.; Anila, E.I. Polypyrrole-silver nanocomposite for enhanced photocatalytic degradation of methylene blue under sunlight irradiation. *Mater. Lett.* **2021**, *298*, https://doi.org/10.1016/j.matlet.2021.130014.
9. Santos, M.C.; Bizeto, M.A.; Camilo, F.F. Polyaniline-niobium oxide nanohybrids with photocatalytic activity under visible light irradiation. *New Journal of Chemistry* **2021**, *45*, 8619-8628, https://doi.org/10.1039/d0nj06215d.
10. Zia, J.; Fatima, F.; Riaz, U. A comprehensive review on the photocatalytic activity of polythiophene-based nanocomposites against degradation of organic pollutants. *Catal. Sci. Technol.* **2021**, *11*, 6630-6648, https://doi.org/10.1039/d1cy01129d.
11. Das, K.K.; Patnaik, S.; Mansingh, S.; Behera, A.; Mohanty, A.; Acharya, C.; Parida, K.M. Enhanced photocatalytic activities of polypyrrole sensitized zinc ferrite/graphitic carbon nitride n-n heterojunction towards ciprofloxacin degradation, hydrogen evolution and antibacterial studies. *J. Colloid Interface Sci.* **2020**, *561*, 551-567, https://doi.org/10.1016/j.jcis.2019.11.030.
12. Wang, D.S.; Wang, Y.H.; Li, X.Y.; Luo, Q.Z.; An, J.; Yue, H.X. Sunlight photocatalytic activity of polypyrrole-TiO2 nanocomposites prepared by 'in situ' method. *Catal. Commun.* **2008**, *9*, 1162-1166, https://doi.org/10.1016/j.catcom.2007.10.027.
13. Liu, Y.; Zhang, H.; Lu, Y.F.; Wu, J.; Xin, B.F. A simple method to prepare g-C(3)N4(/)Ag-polypyrrole composites with enhanced visible-light photocatalytic activity. *Catal. Commun.* **2016**, *87*, 41-44, https://doi.org/10.1016/j.catcom.2016.09.002.
14. Zheng, S.Z.; Zhang, C.Q.; Ma, Y.T.; Qin, F.; Wei, L.; Hu, C.Y. Hierarchical polypyrrole encapsulating Bi2O4 to enhance charge separation and light absorption with boosted visible light photocatalytic activity. *Ceram. Int.* **2021**, *47*, 10574-10581, https://doi.org/10.1016/j.ceramint.2020.12.169.
15. Liu, C.; Chen, F.Y.; Tang, Y.B.; Huo, P.W. An environmentally friendly nanocomposite polypyrrole@silver/reduced graphene oxide with high catalytic activity for bacteria and antibiotics. *J. Mater. Sci.-Mater. Electron.* **2021**, *32*, 15211-15225, https://doi.org/10.1007/s10854-021-06073-4.
16. Ghosh, S.; Keshri, S.R.; Bera, S.; Basu, R.N. Enhanced solar hydrogen generation using Cu-Cu2O integrated polypyrrole nanofibers as heterostructured catalysts", *Int. J. Hydrog. Energy* **2020**, *45*, 6159-6173, https://doi.org/10.1016/j.ijhydene.2019.12.118.
17. Yang, Y.; Ma, S.C.; Qu, J.P.; Li, J.Q.; Liu, Y.; Wang, Q.Q.; Jing, J.; Yuan, Y.; Yao, T.J.; Wu, J. Transforming type-II Fe2O3@polypyrrole to Z-scheme Fe2O3@polypyrrole/Prussian blue via Prussian blue as bridge: Enhanced activity in photo-Fenton reaction and mechanism insight. *J. Hazard. Mater.* **2021**, *405*, https://doi.org/10.1016/j.jhazmat.2020.124668.
18. Sun, X.G.; Liu, Z.; Guo, J.Z.; Li, H.; Wei, D.D.; Li, Z.K.; Zhou, N.; Zhao, T.L.; Yu, G.; Li, Y.T. Novel stable enhanced visible light photocatalytic system based on a Ag3PO4@polypyrrole core-shell Z-scheme with in-situ generated metallic Ag ohmic contacts. *J. Phys. Chem. Solids* **2020**, *146*, https://doi.org/10.1016/j.jpcs.2020.109572.
19. Xie, R.Y.; Fan, J.N.; Fang, K.J.; Chen, W.C.; Song, Y.W.; Pan, Y.; Li, Y.Z.; Liu, J.X. Hierarchical Bi2MoO6 microsphere photocatalysts modified with polypyrrole conjugated polymer for efficient decontamination of organic pollutants. *Chemosphere* **2022**, *286*, https://doi.org/10.1016/j.chemosphere.2021.131541.

20. Li, S.; Zeng, H.Y.; Xiong, J.; Xu, S. Polypyrrole decorated ZnTi hydrotalcite with enhanced adsorption and Cr(VI) photoreduction activity under visible-light. *Adv. Powder Technol.* **2021**, *32*, 3090-3100, https://doi.org/10.1016/j.apt.2021.06.021.
21. Sagadevan, S.; Lett, J.A.; Weldegebrieal, G.K.; Imteyaz, S.; Johan, M.R. Synthesis, characterization, and photocatalytic activity of PPy/ SnO2 nanocomposite. *Chem. Phys. Lett.* **2021**, *783*, https://doi.org/10.1016/j.cplett.2021.139051.
22. Lv, K.L; Wan, D.T.; Zheng, D.Z.; Qin, Y.S.; Lv, Y. Enhancement of visible light photocatalytic activity of BiVO4 by polypyrrole modification. *J. Alloy. Compd.* **2021**, *872*, https://doi.org/10.1016/j.jallcom.2021.159597.
23. Thwala, M.M.; Dlamini, L.N. Photocatalytic reduction of Cr(VI) using Mg-doped WO3 nanoparticles. *Environ. Technol.* **2020**, *41*, 2277-2292, https://doi.org/10.1080/09593330.2019.1629635.
24. Cai, J.; Wu, X.; Li, S.; Zheng, F. Synthesis of TiO2@WO3/Au Nanocomposite Hollow Spheres with Controllable Size and High Visible-Light-Driven Photocatalytic Activity. *ACS Sustain. Chem. Eng.* **2016**, *4*, 1581-1590, https://doi.org/10.1021/acssuschemeng.5b01511,
25. Harshulkhan, S. M.; Janaki, K.; Velraj, G.; Ganapthy, R. S.; Nagarajan, M. Effect of Ag doping on structural, optical and photocatalytic activity of tungsten oxide (WO3) nanoparticles. *J. Mater. Sci.-Mater. Electron.* **2016**, *27*, 4744-4751, https://doi.org/10.1007/s10854-016-4354-3.
26. Mohammadi, S.; Sohrabi, M.; Golikand, A.N.; Fakhri, A. Preparation and characterization of zinc and copper co-doped WO3 nanoparticles: Application in photocatalysis and photobiology. *J. Photochem. Photobiol. B-Biol.* **2016**, *161*, 217-221, https://doi.org/10.1016/j.jphotobiol.2016.05.020.
27. Xekoukoulotakis, N. P.; Mantzavinos, D.; Bahnemann, D. Synthesis and photocatalytic activity of boron-doped TiO2 in aqueous suspensions under UV-A irradiation. *Water Sci. Technol.* **2010**, *61*, 2501-2506, https://doi.org/10.2166/wst.2010.150.
28. Kim, S.; Yoon, H.; Kim, D. Y.; Kim, S.O.; Leem, J.Y. Optical properties and electrical resistivity of boron-doped ZnO thin films grown by sol–gel dip-coating method. *Opt. Mater.* **2013**, *35*, 2418-2424, https://doi.org/10.1016/j.optmat.2013.06.048.
29. Liu, Z.S.; Liu, J.L.; Niu, J.N. Boron-doped bismuth oxybromide microspheres with enhanced surface hydroxyl groups: Synthesis, characterization and dramatic photocatalytic activity. *J. Colloid Interface Sci.* **2016**, *463*, 324-331, https://doi.org/10.1016/j.jcis.2015.10.028.
30. Kuo, C.Y.; Wu, C.H.; Hsu, M.J. Single-step solvothermal synthesis of boron-doped Bi2WO6 visible-light-induced photocatalyst and determination of surface characteristics and photocatalytic activities. *esalin. Water Treat.* **2017**, *81*, 209-215, https://doi.org/10.5004/dwt.2017.21184.
31. Thilagavathi, T.; Venugopal, D.; Marnadu, R.; Chandrasekaran, J.; Alshahrani, T.; Shkir, M. An Investigation on Microstructural, Morphological, Optical, Photoluminescence and Photocatalytic Activity of WO(3) for Photocatalysis Applications: An Effect of Annealing. *J. Inorg. Organomet. Polym. Mater.* **2021**, *31*, 1217-1230, https://doi.org/10.1007/s10904-020-01731-2.
32. Stejskal, J.; Sapurina, I.; Vilcakova, J.; Plachy, T.; Sedlacik, M.; Bubulinca, C.; Goralik, M.; Trchova, M.; Kolska, Z.; Prokes, J. Conducting and Magnetic Composites Polypyrrole Nanotubes/Magnetite Nanoparticles: Application in Magnetorheology. *ACS Appl. Nanomater.* **2021**, *4*, 2247-2256, https://doi.org/10.1021/acsanm.1c00063.
33. Basumatary, B.; Basumatary, R.; Ramchiary, A.; Konwar, D. Evaluation of Ag@TiO2/WO3 heterojunction photocatalyst for enhanced photocatalytic activity towards methylene blue degradation. *Chemosphere* **2022**, *286*, https://doi.org/10.1016/j.chemosphere.2021.131848.
34. Neto, N.F.A.; Zanatta, P.; Nascimento, L.E.; Nascimento, R.M.; Bomio, M.R.D.; Motta, F.V. Characterization and Photoluminescent, Photocatalytic and Antimicrobial Properties of Boron-Doped TiO2 Nanoparticles Obtained by Microwave-Assisted Solvothermic Method. *J. Electron. Mater*. **2019**, *48*, 3145-3156, https://doi.org/10.1007/s11664-019-07076-y.
35. Zerjav, G.; Arshad, M.S.; Djinovic, P.; Zavasnik, J.; Pintar, A. Electron trapping energy states of TiO2-WO3 composites and their influence on photocatalytic degradation of bisphenol A. *Appl. Catal. B-Environ.* **2017**, *209*, 273-284, https://doi.org/10.1016/j.apcatb.2017.02.059.
36. Jia, J.; Taniyama, K.; Imura, M.; Kanai, T.; Shigesato, Y. A visible-light active TiO2 photocatalyst multilayered with WO3. *Phys. Chem. Chem. Phys.* **2017**, *19*, 17342-17348. https://doi.org/10.1039/c7cp03291a.
37. Hasan, J.; Li, H.; Tian, G.; Qin, C. Fabrication of Cr2S3-GO-TiO2 composite with high visible-light-driven photocatalytic activity on degradation of organic dyes. *Chem Phys.* **2020**, *539*, https://doi.org/10.1016/j.chemphys.2020.110950.